Published in final edited form as:
Magn Reson Med. 2010 April ; 63(4): 922–929. doi:10.1002/mrm.22229.

High-Resolution Magnetic Resonance Colonography and Dynamic Contrast-Enhanced Magnetic Resonance Imaging in a Murine Model of Colitis

Devkumar Mustafi[1,*], **Xiaobing Fan**[2], **Urszula Dougherty**[3], **Marc Bissonnette**[3], **Gregory S. Karczmar**[2], **Aytekin Oto**[2], **John Hart**[4], **Erica Markiewicz**[2], and **Marta Zamora**[2]

[1] Department of Biochemistry and Molecular Biology, The University of Chicago, Chicago, Illinois, USA

[2] Department of Radiology, The University of Chicago, Chicago, Illinois, USA

[3] Department of Medicine, The University of Chicago, Chicago, Illinois, USA

[4] Department of Pathology, The University of Chicago, Chicago, Illinois, USA

Abstract

Inflammatory bowel disease, including ulcerative colitis, is characterized by persistent or recurrent inflammation and can progress to colon cancer. Colitis is difficult to detect and monitor noninvasively. The goal of this work was to develop a preclinical imaging method for evaluating colitis. Herein, we report improved MRI methods for detecting and characterizing colitis noninvasively in mice, using high-resolution in vivo MR images and dynamic contrast-enhanced MRI studies, which were confirmed by histologic studies in a murine model of colitis. C57Bl6/J male mice were treated with 2.5% dextran sulfate sodium in their drinking water for 5 days to induce colitis. MR images were acquired using a 9.4-T Bruker scanner from 5–25 days following dextran sulfate sodium treatment. In dynamic contrast-enhanced MRI studies, Gd uptake (K^{trans}) and its distribution (v_e) were measured in muscle and normal and inflamed colons after administering Gd-diethyltriaminepentaacetic acid (Gd-DTPA). T_2-weighted MR images distinguished normal colon from diffusely thickened colonic wall occurring in colitis ($P < 0.0005$) and correlated with histologic features. Values of K^{trans} and v_e obtained from dynamic contrast-enhanced MRI were also significantly different in inflamed colons compared to normal colon ($P < 0.0005$). The results demonstrate that both T_2-weighted anatomic imaging and quantitative analysis of dynamic contrast-enhanced MRI data can successfully distinguish colitis from normal colon in mice.

Keywords

dextran sulfate sodium-induced colitis; dynamic contrast-enhanced MRI; MRI and histology correlation; murine model of colitis; quantitative pharmacokinetic analysis of DCEMRI

Inflammatory bowel disease, which includes ulcerative colitis (1), is characterized by persistent or recurrent inflammation. Ulcerative colitis increases the risk of developing colon cancer. Colitis, in particular the early stages of inflammatory change, is difficult to detect and monitor noninvasively. Improved imaging could allow physicians to monitor colitis

[*]Correspondence to: Devkumar Mustafi, Ph.D., Department of Biochemistry and Molecular Biology, 929 East 57th Street, GCIS-W125M, Chicago, IL 60637-1454. dmustafi@uchicago.edu.

during therapy, determine therapies that work best for individual patients, and also guide the development of new therapies for colitis based on preclinical and clinical research.

Ulcerative colitis is characterized pathologically by mucosal inflammation and moderate to extensive ulceration. Inflammation predominantly affects the mucosa and almost always involves the distal left colon, but it can also extend throughout the colon. Although the etiology of the disease remains unclear, it is believed that an environmental insult such as infection triggers the disease, which involves dysregulated immunologic responses, in genetically susceptible individuals (2). In general, diagnosis of the illness is based on clinical characteristics and endoscopic and histologic mucosal features. Colonoscopy allows direct visualization of the colonic mucosa, the target of the disease. A particular advantage of colonoscopy is that biopsies can be obtained during the examination. Colonoscopies are invasive, however, and can cause complications, including preparation and procedural discomfort, as well as bleeding and perforation. Therefore, the development of improved noninvasive imaging techniques may provide a better surrogate for invasive colonoscopy to facilitate monitoring the disease in early stages and to further advance disease characterization.

Cross-sectional imaging techniques, in particular CT and sonography, are commonly utilized for assessing the extent and severity of inflammatory diseases in the small bowels and the colon; these techniques are also used for planning therapy (3–6). Although CT is a highly sensitive method for detecting intramural disease, as well as extraluminal extension of colonic disease, CT is not recommended as a primary means of diagnosing ulcerative colitis because of its low diagnostic sensitivity for the early disease state (3). In fact, CT cannot detect subtle, superficial mucosal changes revealed on barium studies (4). In addition, repeated CT scans raise a legitimate concern for increased risk of malignancy (7). Recently, MRI has emerged as a valuable tool in detecting abnormalities and assessing disease activity in inflammatory bowel disease and colitis (8–11).

MRI is a cross-sectional technique that produces three-dimensional images, which can reliably detect luminal and extramural lesions. MRI has several advantages compared to CT, including absence of ionizing radiation, superior spatial resolution, higher contrast-to-noise ratio, and ability to perform real-time and functional imaging. The last decade has seen dramatic technical developments, making MRI increasingly attractive as a clinical imaging modality for the abdomen (e.g., Martin et al (8) and references therein). Based on T_1-, T_2-weighted and dynamic contrast-enhanced MRI (DCEMRI), several studies have shown that MRI can be used as a sensitive method to detect inflammation in the small intestine and colon (8–11). Although these studies have shown that DCEMRI is an important technique for differentiating between normal and diseased states, quantitative assessments of contrast enhancement patterns were lacking in these previous works (9–11). In a recent study, we used a pharmacokinetic approach to model DCEMRI data for assessing bowel inflammation in patients with Crohn's disease (12). However, success was modest in that feasibility study because of a small number of subjects, relatively low temporal resolution (as high as 12 sec), and limited acquisition time (4–7 min) (12).

Preclinical animal models are essential for developing new technologies and for defining their potential and limitations. Animal models have been widely used to study potential therapies for colitis and to understand its pathogenesis (13–15). Murine models of colitis also provide an experimental framework to evaluate the efficacy of MRI as an alternative diagnostic method for the early detection and quantitative assessment of inflammation. Administration of dextran sulfate sodium (DSS) in drinking water induces a dose-dependent and time-dependent reversible form of chemical colitis in mice. The clinical and histologic features of this model are well characterized (13–15). However, there have been few in vivo

MRI studies that have examined colitis (16–18) and colorectal tumors in mice (18–20) using anatomic T_2-weighted MR images. Furthermore, there have been no quantitative analyses of contrast enhancement using DCEMRI to assess disease activity or to distinguish inflamed colon from normal colon.

Herein, we report the development of improved MRI methods for detecting and characterizing colitis noninvasively in a clinically relevant murine model, using high-resolution T_2-weighted MR images and DCEMRI studies with intravenous Gd-diethylenetriaminepentaacetic acid (Gd-DTPA). We compared our MRI findings to histologic features in normal colons and colons with active colitis. Using measurements of colon wall thickness and T_2 times of skeletal muscle and colonic tissues, we were able to successfully distinguish normal colon from inflamed colon. In addition, we also established semiquantitative kinetic parameters that characterized and distinguished normal colon from inflamed states using DCEMRI studies. Abnormalities detected by high-resolution MR images correlated closely in temporal and spatial regard with abnormal histologic features of mucosal ulceration and edema in DSS-induced colitis.

MATERIALS AND METHODS

Animal Model

Animal protocols were approved by the Institutional Animal Care and Use Committee of the University of Chicago. Pathogen-free C57Bl6/J male mice were purchased from the Jackson Laboratory (Bar Harbor, ME; weight, 15–20 g). The mice were allowed to habituate for 2 weeks before the study was initiated. Thirty C57Bl6/J male mice were included in this study. For inducing colitis, mice (n = 15) were given 2.5% (weight/volume) DSS (MP Biomedical LLC, Solon, OH; molecular weight, 36,000–50,000) in their drinking water for 5 days, followed by regular water (21), while control mice (n = 15) were given regular water. DSS-treated mice developed clinical colitis with diarrhea, heme occult–positive stools, and weight loss.

In Vivo MRI

MRI studies were performed using a Bruker Biospec (Billerica, MA) 33-cm horizontal-bore scanner with 12-cm-bore, high-performance, self-shielded gradients (maximum gradient strength, 100 mT m^{-1}) at 9.4 T. A custom-designed half birdcage coil (35 mm) was used for in vivo imaging. Animals were anesthetized during procedures with 1.5–2% isoflurane mixed with medical air to maintain a surgical plane of anesthesia. No paralytic agents were used. Temperature was monitored continuously by a thermometer and controlled with warm air. Heart rate, respiration rate, and blood pressure were monitored with an optical detection system from SA Instruments (Stony Brook, NY), developed for use in MRI. A standard 24-gauge intravenous catheter was inserted into the tail vein for injection of Gd-DTPA contrast agent.

High-resolution MR images were acquired with multislice gradient echo and spin echo sequences in both coronal and axial orientations. The parameters for in vivo MRI measurements were as follows: for spin echo images, a fast spin echo sequence with four echoes per excitation (i.e., four phase-encoding steps per excitation; a rapid acquisition with relaxation enhancement sequence), pulse repetition time (TR)/echo time (TE) = 4000/27 msec; array size = 256 × 256; field of view = 30 mm × 30 mm; readout bandwidth = 50 kHz; slice thickness/slice separation = 1.0/1.0 mm; slices = 17 in the coronal plane and 27 in the axial plane; average = 2; and in-plane resolution = 0.117 mm. For gradient echo (a fast low-angle shot sequence); TR/TE = 750/5 msec, flip angle = 30°, while all other parameters were as in the spin echo sequence.

T_1 and T_2

Spin-lattice relaxation (T_1) and spin-spin relaxation (T_2) times were determined based on acquisitions with a saturation recovery sequence and a multislice-multiecho sequence, respectively. For measurements of T_1 values, the parameters were TRs of 100, 200, 500, 750, 1000, 2000, 3000, 5000, 10,000, and 15,000 msec; TE = 10 msec; array size = 128 × 128; slices = 3 in the axial plane; flip angle = 90°; average = 1; and in-plane resolution = 0.234 mm. For measurements of T_2 values, the parameters were TR = 4000 msec, with varying TE from 10 to 400 msec; other parameters were the same as for T_1 measurements. Regions of interest were selected for muscle, normal colon, and inflamed colons to determine their T_1 and T_2 values; the following equations were used: $I_z = I_0\,[1 - \exp(-\mathrm{TR}/T_1)]$ for T_1 and $I_{x,y} = I_0[\exp(-\mathrm{TE}/T_2)]$ for T_2. The values of T_1 and T_2 were calculated from plots of measured intensities (I_z or $I_{x,y}$) as a function of TR or TE values, respectively; a single exponential fit in each case was sufficient.

DCEMRI

DCEMRI covering three central slices (TR/TE = 40/4.5 msec, matrix size = 128 × 128, flip angle = 30°, slice thickness = 1mm) were acquired with a temporal resolution of 5 sec for approximately 12 min. A typical dose of 0.13 mmol/kg of the body weight of Gd-DTPA (OMNISCAN®; GE Healthcare, Princeton, NJ) contrast agent was injected via the catheter during MRI experiments. Approximately 0.2 mL of OMNISCAN was injected intravenously over a period of 5 sec during DCEMRI scans.

Two-Compartment Model

A simple two-compartment model (TCM) composed of intravascular versus extravascular extracellular space was used to describe the distribution of OMNISCAN after bolus injection (22,23). Specifically, the model predicts the change in contrast concentration as a function of time in the tissue C(t) as follows:

$$\frac{dC(t)}{dt} = K^{\mathrm{trans}} \cdot (C_p(t) - C(t)/v_e) \qquad [1]$$

where K^{trans} (min^{-1}) is the volume transfer constant between intravascular and extravascular extracellular space, v_e is the volume of extravascular extracellular space per unit volume of tissue and $C_p(t)$ is the arterial input function. The contrast concentration curves as function of time, C(t), were converted from signal intensity curves for each region of interest by using an approximation with muscle as a reference tissue, as previously published (24). The selections of inflamed colonic segments were based on contrast-enhanced MR images of control and colitis-bearing mice; specifically, on the different T_2 values characteristic of normal colons and inflamed colons. A radiologist (A.O.) and an experienced MR physicist (X.F.) placed regions of interest on colonic segments based on areas of noticeable changes in contrast enhancement. Regions of interest were carefully traced to minimize the partial-volume effects. For analyzing DCEMRI datasets, we used the following measured parameters: a T_1 value of 2000 msec for muscle or colonic tissue and a relaxivity (r_1) of 3.34 × 0.03 $\mathrm{mM}^{-1}\,\mathrm{sec}^{-1}$ for OMNISCAN; these values were carefully measured at 9.4 T.

Empiric Mathematical Model

To compare with the TCM analysis, an empiric mathematical model (EMM) (25) with four parameters was used to fit the same contrast concentration curves as the TCM:

$$C(t) = A \cdot (1 - e^{-\alpha t})^q \cdot e^{-\beta t}, \qquad [2]$$

where A is the upper limit of the tracer concentration, α is the rate of the contrast uptake (min^{-1}), β is the rate of the contrast washout (min^{-1}), and q is related to the slope of early uptake.

Semiquantitative Parameters From EMM

In addition to kinetic parameters obtained from TCM and EMM, semiquantitative parameters including initial area under the curve, initial slope of enhancement between 0 and 1 min ($Slope_{ini}$), and the time to peak enhancement (T_{peak}) were calculated based on analyses of EMM. These semiquantitative diagnostic parameters can be derived from the primary EMM parameters as follows:

Initial Area Under the Curve—Initial area under the curve values were calculated using the numerical integral over the EMM from 0 to τ min: $\mathrm{IAUC}=\int_0^\tau A\cdot(1-e^{-\alpha t})^q\cdot e^{-\beta t}dt$. The value of τ = 1 min was selected for this study.

Initial Enhancement Slope Between Time 0 and 1 Min—Initial enhancement was determined by using the formula to calculate the slope of the line containing these two points on the curve: $Slope_{ini} = A\cdot(1-e^{-\alpha})^q\cdot e^{-\beta}$.

Time to Peak of Enhancement (T_{peak})—T_{peak} values were estimated by directly adopting the formula derived by Fan et al. (26): $T_{peak}=\frac{1}{\alpha}\log\left(1+\frac{q\alpha}{\beta}\right)$.

Data and Statistical Analysis

All data analyses were performed with computer programs written in IDL (Research Systems, Inc., Boulder, CO). The average signal intensities over the regions of interest were calculated to generate signal intensity time curves, which were then converted to contrast concentration curves. The goodness-of-fit parameter, R_2, was calculated for each curve to determine how well the TCM and EMM fitted the measured kinetic data.

All parameters were compared between normal and inflamed colonic segments. Average values with standard deviations were calculated, and Student t tests were performed between normal and inflamed colonic segments. A confidence interval of $P < 0.0005$ was considered statistically significant.

Tissue Harvesting and Immunohistochemistry

Following in vivo MRI studies (at day = 12 following DSS treatment for colitis-bearing subjects), mice were sacrificed and colons were harvested. Colonic sections with colitis (n = 5) and normal colon tissue (n = 5) were excised for histology. Colons were fixed flat in 10% buffered formalin for 24 h and paraffin embedded as Swiss rolls. Colonic Swiss roll segments (5 μm) were stained with hematoxylin and eosin and evaluated for inflammation, edema, and ulceration by a gastrointestinal pathologist (J.H.), as previously described (21). We have correlated the MR findings, based on both T_2-weighted and DCEMR images, with histologic features. The comparisons were based on distal colonic segments, corroborated with high-resolution photographs of the excised colons, MR images, and histologic features.

RESULTS

Figure 1a illustrates how mice were positioned inside a coil of ~35mm in size for in vivo imaging. The blue arrows indicate a typical abdominal area—from the rectum to the diaphragm—that was imaged in this study. MR images of a control mouse and a colitis-bearing mouse, acquired in the coronal plane, are shown in Fig. 1b and c. The white arrows

in Fig. 1b indicate an empty, air-filled colon, while the yellow arrows in Fig. 1c indicate an inflamed colon. As seen in Fig. 1c, the inflamed colon appears much thicker and much brighter than a normal colon. In Fig. 1b1 and c1, adjacent to MR images, high-resolution photographs of the corresponding excised colons are also shown. In the normal colon, the mucosa was transparent, while the excised colon with colitis was ulcerated, with scattered islands of residual mucosa.

Figure 2 compares in vivo MR images of colons of a control mouse (Fig. 2a and b, a gradient echo image and a spin echo image, respectively) and a colitis-bearing mouse (Fig. 2c1–c3 and d1–d3) as a function of the number of days following DSS treatment. The gradient echo and spin echo MR images of a colitis-bearing mouse, acquired at day 5 in Fig. 2c1 and d1, day 12 in Fig. 2c2 and d2, and day 25 in Fig. 2c3 and d3, are shown. The thin colonic wall of a control mouse and the inflamed colon of a colitis-bearing mouse are indicated by arrows in Fig. 2. The markedly thickened colonic walls in a colitis-bearing mouse, particularly at day 5 (Fig. 2c1 and d1) and day 12 (Fig. 2c2 and d2) are indicative of marked bowel wall edema. The colonic inflammation at day 25 (Fig. 2c3 and d3) is still visible and is seen as brighter circles in MR images, indicated by arrows.

In Table 1, we listed values of spin-lattice relaxation times (T_1) and spin-spin relaxation times (T_2) of skeletal muscle and colonic tissues, and of colon wall thickness of normal and colitis-bearing mice. T_1 values of muscle, normal colon, and inflamed colon (~2–2.3 sec) could not be distinguished between different tissues, and differences between them were not statistically significant. On the other hand, T_2 relaxation times, as measured by MRI, for skeletal muscle, normal colon, and inflamed colon tissues were significantly different. For colitis, T_2 value increased ~80% compared to normal colon with $P < 0.0005$. Table 1 also compares values of colon wall thickness as measured by MRI for control and colitis-bearing mice. The thickness of colonic wall increased about 4- and 10-fold in colitis-bearing mice at day 5 and day 12, respectively, compared to normal colon ($P < 0.0005$), as is evident in MR images in Figs. 1 and 2.

Figure 3 shows contrast uptake curves for inflamed colon, normal colon, and skeletal muscle, obtained from DCEMRI studies after injecting a dose of 0.13 mmol/kg of Gd-DTPA. Analyses of contrast uptake and washout kinetics were performed based on two independent models of TCM and EMM. We analyzed DCEMRI datasets to measure contrast concentration as a function of time in regions of interest within colonic segments and skeletal muscle, as shown in Fig. 3. Fits to the contrast uptake curves with both TCM and EMM are also shown by solid lines in green and red, respectively. As seen in Fig. 3, the contrast uptake curve for muscle tissues in either normal mice or in colitis-bearing mice was well approximated with both models. However, EMM provided better fits for normal and inflamed colons over TCM fits.

Table 2 lists the average values with standard deviations of kinetic parameters that were obtained from fits to TCM and EMM, as well as values of semiquantitative parameters that resulted from analyses of EMM. From TCM fits, the values of K^{trans} and v_e were determined for skeletal muscle and colon tissues in the control group and the colitis group. In muscle, the corresponding values exhibited no differences between the two groups. On the other hand, for normal and inflamed colons the values of K^{trans} and v_e in the colitis group increased almost 2-fold compared to that of the control group ($P < 0.0005$). A similar analysis from EMM exhibited increased contrast uptake (A), larger value of the initial area under the curve, steeper enhancement slope ($Slope_{ini}$), and increased time-to-peak enhancement (T_{peak}) for the colitis group compared to that of the control group ($P < 0.0005$). Values of three other parameters, α, β, and q, were lower in the colitis group than in the control group, but they were not statistically significant. The analysis from EMM for

skeletal muscle between the two groups demonstrated a decreased rate of contrast medium washout (β) and an increased T_{peak} in the colitis group compared to that of the control group ($P \leq 0.001$). Finally, in contrast to skeletal muscle, the goodness-of-fit parameter, R^2, was higher in EMM compared to TCM in colonic tissue (0.97 versus 0.88), suggesting EMM provided a better fit to the contrast concentration curves, as seen in Fig. 3.

Figure 4 compares hematoxylin and eosin–stained sections of Swiss rolls of normal colon from a control mouse and inflamed colon from a DSS-treated mouse on day 12. In Fig. 4a, the histologic features of normal mucosa, submucosa, and muscle layers are seen. In Fig. 4b, colonic segments from a DSS-treated mouse that differ in inflammation and edema are shown. An area with relatively healed epithelium and normal bowel wall thickness is indicated by white arrows. In another area, yellow arrows indicate a colonic segment with complete ulceration of the mucosa, replaced by granulation tissue overlying markedly edematous smooth muscle layers. The colonic wall in this area was markedly thickened compared to normal or healed colonic segments.

DISCUSSION

The goal of this work was to develop improved preclinical imaging tools for gastrointestinal research. Furthermore, we wanted to make these valuable new imaging tools available to the scientific and clinical communities. To achieve our primary objective, we approached the problem based on two central assumptions. First, since colitis is characterized by increased edema, we speculated that the increased water content in mucosal and submucosal layers should be detected in noncontrast, T_2-weighted images (27–29). Second, bowel wall edema would be expected to cause a relative decrease in blood vessel density, while inflammation might alter blood flow by vasomotor mechanisms (30). The net effect of these changes is hard to predict a priori, but we theorized that they might alter the kinetics of uptake and washout in inflamed colon compared to normal colon (30,31). Therefore, we examined the kinetics of uptake and washout of contrast agents using DCEMRI to assess its ability to discriminate the diseased state (colitis) from the normal state. Furthermore, if imaging parameters could be developed that would differentiate diseased from normal colon in a preclinical setting, this knowledge might then be clinically applied to human subjects to improve early diagnosis and to assess changes in the degree of disease activity.

We demonstrated that MRI can be used as a noninvasive technique to quantitatively characterize colitis in a murine model. The markedly thickened colon wall in the DSS colitis model reflects increased bowel wall edema and inflammatory activity, as demonstrated by T_2-weighted MR images and confirmed by histologic sections. Increased colon wall thickness in a colitis model, as assessed by MRI, has also been documented by other investigators (16–18). We have extended these studies and, for the first time, quantitatively characterized relaxation parameters for skeletal muscle, normal colon, and inflamed colon. T_1 values could not be used to distinguish these tissues, whereas T_2 values clearly differentiated normal from diseased colon ($P < 0.0005$). The increased discriminating ability of T_2-weighted images derives from the increased water signal arising from edema in the inflamed colon. The contribution of ulceration will require further study as ulceration is always accompanied by bowel wall edema in colitis. Nonetheless, these results from noncontrasted, T_2-weighted MRI are indeed very promising as a noninvasive method to detect early stages of disease and to differentiate colitis from normal colon.

Our results also demonstrated that DCEMRI can be successfully used as a quantitative assessment of colonic inflammation in ulcerative colitis. To the best of our knowledge, such an assessment of colitis severity in a murine model using DCEMRI has not been previously reported. Based on “TCM analyses”, inflamed colonic segments exhibited a faster volume

transfer rate (K^{trans}) and a larger volume of distribution of contrast medium (v_e) when compared to normal colons, as seen in Fig. 3 and Table 2. Based on semiquantitative analyses using EMM, the inflamed colonic segments were characterized by increased contrast uptake, higher IUAC, steeper initial enhancement slopes, and a longer duration for time-to-peak contrast enhancement compared to normal colons ($P < 0.0005$). These two independent models are in excellent agreement with respect to their analyses of kinetic parameters. These analyses, based on pharmacokinetic modeling of contrast kinetics, have identified significant changes in the functional vascular compartment in diseased colon compared to normal colon. The individual contributions of alterations in blood flow and changes in vessel density in the bowel wall will require careful morphometric studies of perfused colons.

While the inflamed colon showed an increased initial rate of Gd uptake compared to normal colon, the contrast medium washout profile in both colitis and normal colon appeared to be very similar. The washout rates, β, in the two groups were identical and very slow. This might be due to the leaky vasculature and a heterogeneous microenvironment. Once Gd leaks out from the vessels, its retention time in edematous mucosa and submucosa layers appears to be longer than that of other tissue types, e.g., muscle. Because of the slower washout rate of Gd, the EMM provided better fits than the TCM, as shown in Fig. 3 and as indicated by the values of R^2, listed in Table 2. It is also of interest to point out that the Gd washout rate in skeletal muscle of colitis-bearing mice was significantly slower compared to that of the control group ($P \leq 001$). To the best of our knowledge, we have not seen this observation reported in the literature. Several explanations might be offered for this phenomenon, including local extension of inflammation or systemic effects of colitis on blood vessel permeability in adjacent muscle.

Brahme and Lindstrom (30) reported a comparative radiographic and pathologic study of intestinal vascular architecture in Crohn's disease and ulcerative colitis. It has been shown that normal colon contains small-caliber blood vessels in lamina propria and submucosa, whereas tissues with Crohn's disease or ulcerative colitis contain numerous dilated vessels (30,31). In active ulcerative colitis, hypervascularity is more prevalent than in Crohn's disease but is confined to the mucosa and adjacent submucosa (30). Increased vascularity and edematous mucosa in ulcerative colitis correlate with the level of colonic inflammation and the severity of the disease (31). We demonstrated increased Gd contrast uptake in inflamed colon by quantitative DCEMRI using both models of TCM and EMM. Furthermore, the increased T_2 values and colon wall thickness in inflamed colons reflect increased water content from colitis-associated edema, which we confirmed in our histologic correlations. The excellent correlation of quantitative parameters obtained from MRI with underlying disease anatomy and physiology suggests that MRI could have a critical role for monitoring disease activity and evaluating responses to clinical therapy.

We recently reported a pilot study using quantitative kinetic parameters derived from DCEMRI to assess bowel inflammation in Crohn's disease (12). Although there were some limitations in the pilot study, including a small number of subjects, the findings were consistent with results obtained in this current report. The human studies, taken together with results presented in this report on a murine disease model, suggest that high-resolution MR enterography, in conjunction with DCEMRI studies, could provide a useful diagnostic imaging tool for early detection and accurate assessment of inflammation in the small bowel and colon. Since the DSS model of colitis exhibits several features in common with human colitis, including bowel wall edema and inflammation, our preclinical findings have important translational implications for its application in the clinical setting. Controlled clinical studies correlating endoscopic and MRI findings in patients should be recommended.

Inflammation in ulcerative colitis is increasingly recognized as causally important in neoplastic progression (32). Thus, an important challenge is to distinguish colitis from colon cancer in the background of ulcerative colitis. Since the present study demonstrates that we can quantitatively evaluate colitis in mice based on T_2-weighted MR images and DCEMRI data using both TCM and EMM, the primary goal of our future studies will be to develop a high-resolution MRI method for assessing the state of colitis and to facilitate the early detection of colitis-associated colorectal tumors in mice.

Acknowledgments

Grant sponsor: American Cancer Society, Illinois Division; Grant number: 08-45.

Grant sponsor: National Institutes of Health; Grant numbers: NCI:2RO1 CA36745, NIBIB:R33 CA100996.

Grant sponsor: Digestive Diseases Research Core Center Grant at the University of Chicago; Grant number: P30 DK42086.

This work was partially supported by the Lynn S. Florsheim MRIS facility.

References

1. Strober W, Fuss I, Mannon P. The fundamental basis of inflammatory bowel disease. J Clin Invest. 2007; 117:514–521. [PubMed: 17332878]
2. Bouma G, Strober W. The immunological and genetic basis of inflammatory bowel disease. Nat Rev Immunol. 2003; 3:521–533. [PubMed: 12876555]
3. Gore RM, Balthazar EJ, Ghahremani GG, Miller FH. CT features of ulcerative colitis and Crohn's disease. AJR Am J Roentgenol. 1996; 167:3–15. [PubMed: 8659415]
4. Thoeni RF, Cello JP. CT imaging of colitis. Radiology. 2006; 240:623–638. [PubMed: 16926320]
5. Pradel JA, David XR, Taourel P, Djafari M, Veyrac M, Bruel JM. Sonographic assessment of the normal and abnormal bowel wall in nondiverticular ileitis and colitis. Abdom Imaging. 1997; 22:167–172. [PubMed: 9013527]
6. Limberg B, Osswald B. Diagnosis and differential diagnosis of ulcerative colitis and Crohn's disease by hydrocolonic sonography. Am J Gastroenterol. 1994; 89:1051–1057. [PubMed: 8017364]
7. Sadetzki S. Excess lifetime cancer mortality risk attributed to radiation exposure from pediatric computed tomography scan. Isr Med Assoc J. 2007; 9:607–609. [PubMed: 17877069]
8. Martin DR, Lauenstein T, Sitaraman SV. Utility of magnetic resonance imaging in small bowel Crohn's disease. Gastroenterology. 2007; 133:385–390. [PubMed: 17681157]
9. Florie J, Wasser MNJM, Arts-Cieslik K, Akkerman EM, Siersema PD, Stroker J. Dynamic contrast-enhanced MRI of the bowel wall for assessment of disease in Crohn's disease. AJR Am J Roentgenol. 2006; 186:1384–1392. [PubMed: 16632735]
10. Pupillo VA, Di Cesare E, Frieri G, Limbucci N, Tanga M, Masciocchi C. Assessment of inflammatory activity in Crohn's disease by means of dynamic contrast-enhanced MRI. Radiol Med. 2007; 112:798–809. [PubMed: 17885739]
11. del Vescovo R, Sansoni I, Caviglia R, Ribolsi M, Perrone G, Leoncini E, Grasso RF, Cicala M, Zobel BB. Dynamic contrast enhanced magnetic resonance imaging of the terminal ileum: differentiation of activity of Crohn's disease. Abdom Imaging. 2008; 33:417–424. [PubMed: 17639383]
12. Oto A, Fan X, Mustafi D, Jansen JA, Karczmar GS, Rubin DT, Kayhan A. Quantitative analysis of dynamic contrast enhanced MRI for assessment of bowel inflammation in Crohn's disease: pilot study. Acad Radiol. 10.1016/j.acra.2009.04.010
13. Okayasu I, Hatakeyama S, Yamada M, Ohkusa T, Inagaki Y, Nakaya R. A novel method in the induction of reliable experimental acute and chronic ulcerative colitis in mice. Gastroenterology. 1990; 98:694–702. [PubMed: 1688816]

14. Cooper HS, Murthy SN, Shah RS, Sedergran DJ. Clinicopathologic study of dextran sulfate sodium experimental murine colitis. Lab Invest. 1993; 69:238–249. [PubMed: 8350599]
15. Okayasu I, Ohkusa T, Kajiura K, Kanno J, Sakamoto S. Promotion of colorectal neoplasia in experimental murine ulcerative colitis. Gut. 1996; 39:87–92. [PubMed: 8881816]
16. Larsson AE, Melger S, Rehnstrom E, Michaelsson E, Svensson L, Hockings P, Olsson LE. Magnetic resonance imaging of experimental mouse colitis and association with inflammatory activity. Inflamm Bowel Dis. 2006; 12:478–485. [PubMed: 16775491]
17. Melger S, Gillberg P-G, Hockings PD, Olsson LE. High-throughput magnetic resonance imaging in murine colonic inflammation. Biochem Biophys Res Commun. 2007; 355:1102–1107. [PubMed: 17336266]
18. Young MR, Ileva LV, Bernardo M, Riffle LA, Jones YL, Kim YS, Colburn NH, Choyke PL. Monitoring of tumor promotion and progression in a mouse model of inflammation-induced colon cancer with magnetic resonance colonography. Neoplasia. 2009; 11:237–246. [PubMed: 19242605]
19. Heilmann M, Walczak C, Vautier J, Dimicoli J-L, Thomas CD, Lupu M, Mispelter J, Volk A. Simultaneous dynamic T_1 and T_2* measurements for AIF assessment combined with DCE MRI in a mouse tumor model. MAGMA. 2007; 20:193–203. [PubMed: 17929067]
20. Hensley HH, Chang W-C, Clapper ML. Detection and volume determination of colonic tumors in *Min* mice by magnetic resonance micro-imaging. Magn Reson Med. 2004; 52:524–529. [PubMed: 15334570]
21. Tao Y, Hart J, Lichtenstein L, Joseph LJ, Ciancio MJ, Hu S, Chang EB, Bissonnette M. Inducible heat shock protein 70 prevents multifocal flat dysplasia lesions and invasive tumors in an inflammatory model of colon cancer. Carcinogenesis. 2009; 30:175–182. [PubMed: 19005184]
22. Tofts PS, Brix G, Buckley DL, Evelhoch JL, Henderson E, Knopp MV, Larsson HB, Lee TY, Mayr NA, Parker GJ, Port RE, Taylor J, Weisskoff RM. Estimating kinetic parameters from dynamic contrast-enhanced T(1)-weighted MRI of a diffusable tracer: standardized quantities and symbols. J Magn Reson Imaging. 1999; 10:223–232. [PubMed: 10508281]
23. Brix G, Seminmler W, Port R, Schad LR, Layer G, Lorenz WJ. Pharmacokinetic parameters in CNS Gd(DTPA) enhanced MR imaging. J Comput Assist Tomogr. 1991; 15:621–628. [PubMed: 2061479]
24. Medved M, Karczmar G, Yang C, Dignam J, Gajewski TF, Kindler H, Vokes E, MacEneany P, Mitchell MT, Stadler WM. Semiquantitative analysis of dynamic contrast enhanced MRI in cancer patients: Variability and changes in tumor tissue over time. J Magn Reson Imaging. 2004; 20:122–128. [PubMed: 15221817]
25. Fan X, Medved M, River JN, Zamora M, Corot C, Robert P, Bourrinet P, Lipton M, Culp RM, Karczmar GS. New model for analysis of dynamic contrast-enhanced MRI data distinguishes metastatic from nonmetastatic transplanted rodent prostate tumors. Magn Reson Med. 2004; 51:487–494. [PubMed: 15004789]
26. Fan X, Medved M, Karczmar GS, Yang C, Foxley S, Arkani S, Recant W, Zamora MA, Abe H, Newstead GM. Diagnosis of suspicious breast lesions using an empirical mathematical model for dynamic contrast-enhanced MRI. Magn Reson Imaging. 2007; 25:593–603. [PubMed: 17540270]
27. Maccioni F, Colaiacomo MC, Parlanti S. Ulcerative colitis: value of MR imaging. Abdom Imaging. 2005; 30:584–592. [PubMed: 15886952]
28. Gouya H, Vignaux O, Le Roux P, Chanson P, Bertherat J, Bertagna X, Legmann P. Rapidly reversible myocardial edema in patents with acromegaly: assessment with ultrafast T2 mapping in a single-breath-hold MRI sequence. AJR Am J Roentgenol. 2008; 190:1576–1582. [PubMed: 18492909]
29. Oh J, Cha S, Aiken AH, Han ET, Crane JC, Stainsby JA, Wright GA, Dillon WP, Nelson SJ. Quantitative apparent diffusion coefficients and T2 relaxation times in characterizing contrast enhancing brain tumors and regions of peritumoral edema. J Magn Reson Imaging. 2005; 21:701–708. [PubMed: 15906339]
30. Brahme F, Lindstrom C. A comparative radiographic and pathological study of intestinal vaso-architecture in Crohn's disease and in ulcerative colitis. Gut. 1970; 11:928–940. [PubMed: 5492249]

31. Danse S, Sans M, Motte CDL, Graziani C, West G, Phillips MH, Pola R, Rutella S, Willis J, Gasbarrini A, Fiocchi C. Angiogenesis as a novel component of inflammatory bowel disease pathogenesis. Gastroenterology. 2006; 130:2060–2073. [PubMed: 16762629]

32. Fukata M, Chen A, Vamadevan AS, Cohen J, Breglio K, Krishnareddy S, Hsu D, Xu R, Harpaz N, Dannenberg AJ, Subbaramaiah K, Cooper HS, Itzkowitz SH, Abreu T. Toll-like receptor-4 promotes the development of colitis-associated colorectal tumors. Gastroenterology. 2007; 133:1869–1881. [PubMed: 18054559]

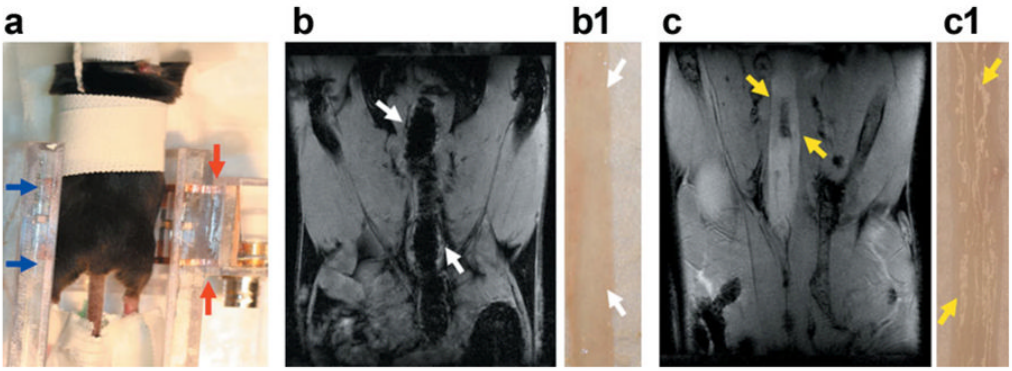

FIG. 1.

In vivo abdominal MR images of mice. **a**: This photograph shows how mice were set up inside a half birdcage coil (35mm in size) for in vivo imaging. The blue arrows indicate the length of the mouse body that can be scanned with this particular coil; the two ends of this coil are indicated by red arrows. **b**: An MR image is shown of a control, male C57Bl6/J mouse in the coronal plane that was acquired with a gradient echo sequence with an in-plane resolution of 117 microns. In this MR image, the air-filled colon is indicated by white arrows. The adjacent panel (**b1**) shows a high-resolution photograph of an excised colon from a control mouse; only the thin translucent wall is seen. **c**: An MR image in the coronal plane is shown of a colitis-bearing mouse; the brighter inflamed colon is markedly thickened, as indicated by yellow arrows. In the adjacent photograph (**c1**), the corresponding excised colon shows a thickened wall, ulcerated with scattered islands of residual mucosa.

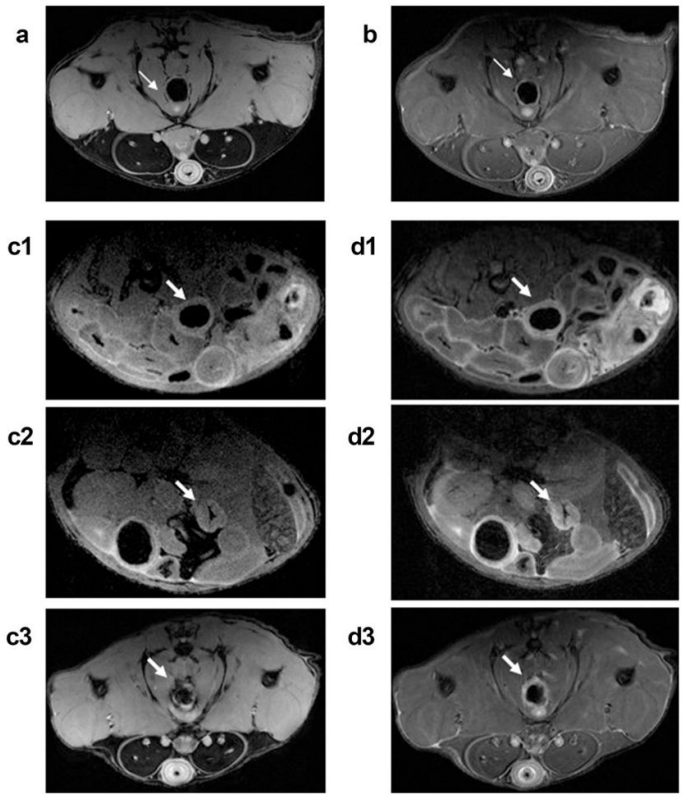

FIG. 2.

In vivo MR images of mouse colons. **a,b**: Gradient echo and spin echo images, respectively, are shown for a control mouse in the axial plane. Gradient echo images of a colitis-bearing mouse that were acquired at day 5 (**c1**), day 12 (**c2**), and day 25 (**c3**) following the DSS treatment are shown. **d1–d3**: The corresponding spin echo images are shown for the same colitis-bearing mouse as in (**c1–c3**). The normal colon in (**a**) and (**b**) is indicted by thin white arrows, while the inflamed colons in (**c1–c3**) and (**d1–d3**) are indicated by thicker white arrows.

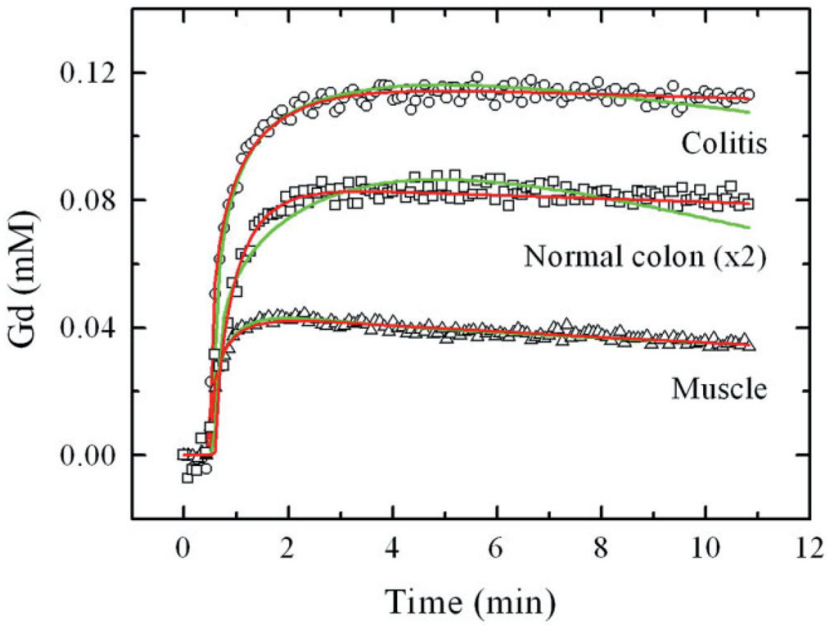

FIG. 3.

Contrast uptake curves for inflamed (colitis) colon, normal colon, and skeletal muscle. From DCEMRI studies, gadolinium uptake (in millimolar) as a function of time (in minutes) is shown for colitis (open circles), normal colon (open squares), and skeletal muscle (open triangle). Since the Gd uptake in normal colon and skeletal muscle overlaps, for visual clarity the scale of Gd enhancement for normal colon was multiplied by 2, indicated in the figure as “normal colon (×2).” Fits to the contrast uptake curves are shown for the TCM (Eq. 1, green line) and an EMM (Eq. 2, red line).

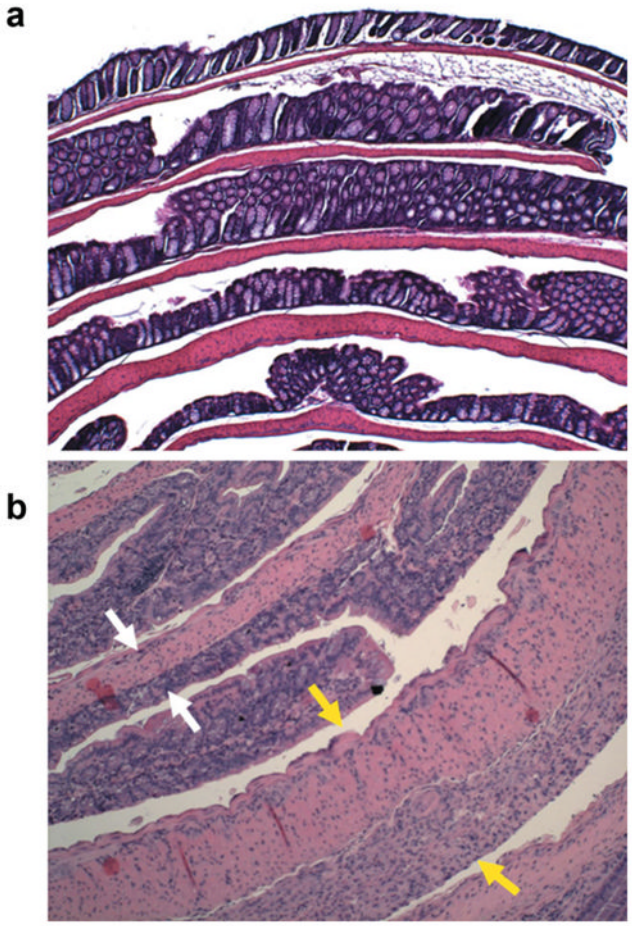

FIG. 4.

Hematoxylin and eosin–stained histologic sections of colons from normal (**a**) and DSS-treated mice (**b**) prepared as Swiss rolls. Both images are displayed in the same scale, ×10. In the inflamed colon, white arrows indicate an area with healed epithelium and normal colon wall thickness. The yellow arrows indicate a colonic segment with complete ulceration. The mucosa is replaced by edematous granulation tissue and the colonic wall is markedly thickened.

Table 1

MRI-Determined Parameters of Spin-Lattice Relaxation Times (T_1), Spin-Spin Relaxation Times (T_2), and Values of Colon Wall Thickness*

Parameters	Muscle	Normal colon	Colitis (colon)	*P* value between colons
T_1 (msec)	1985.9 ± 183.2	2168.6 ± 199.6	2311.6 ± 203.5	0.439
T_2 (msec)	27.4 ± 1.0	39.6 ± 1.7	71.3 ± 2.5	5.41×10^{-5}
Colon wall (mm)	n.d.	0.10 ± 0.02	0.40 ± 0.04 (day 5) 1.01 ± 0.07 (day 12)	3.14×10^{-4} 2.69×10^{-5}

*Estimated values were based on measurements of $n = 10$ of control mice and of $n = 10$ of colitis-bearing mice. The corresponding *P* values are listed between normal colons and colitis-bearing colons.

n.d. - not determined.

Table 2

Summary of Kinetic Parameters Calculated From the TCM and EMM and Semiquantitative Parameters for Normal and Inflamed Colonic Segments and Skeletal Muscle*

Parameter	Muscle from control	Muscle from colitis	*P* value between muscle	Colon from control	Colon from colitis	P value between colons
Two-compartment model (TCM)						
K^{trans}	0.12 ± 0.01	0.11 ± 0.01	0.27	0.12 ± 0.003	0.24 ± 0.01	$<\mathbf{10^{-5}}$
v_e	0.21 ± 0.02	0.20 ± 0.01	0.13	0.37 ± 0.02	0.59 ± 0.04	$<\mathbf{10^{-5}}$
R^2	0.94 ± 0.01	0.95 ± 0.02	n.a.	0.88 ± 0.03	0.89 ± 0.03	n.a.
Empirical mathematical model (EMM)						
A	0.36 ± 0.04	0.37 ± 0.03	0.47	0.33 ± 0.03	1.03 ± 0.08	$<\mathbf{10^{-5}}$
q	0.31 ± 0.08	0.31 ± 0.04	0.89	0.50 ± 0.10	0.33 ± 0.05	0.005
α	2.20 ± 0.44	1.76 ± 0.22	0.04	1.86 ± 0.52	1.06 ± 0.23	0.006
β	0.048 ± 0.013	0.022 ± 0.003	0.001	0.009 ± 0.003	0.007 ± 0.004	0.15
R^2	0.96 ± 0.01	0.98 ± 0.02	n.a.	0.95 ± 0.01	0.99 ± 0.01	n.a.
Semiquantitative analyses						
IAUC[a]	0.28 ± 0.03	0.29 ± 0.03	0.89	0.23 ± 0.02	0.70 ± 0.05	$<\mathbf{10^{-5}}$
$Slope_{ini}$	0.33 ± 0.04	0.34 ± 0.03	0.44	0.30 ± 0.02	0.88 ± 0.06	$<\mathbf{10^{-5}}$
T_{peak}	1.25 ± 0.20	1.87 ± 0.14	$\mathbf{10^{-4}}$	2.57 ± 0.42	3.99 ± 0.80	$\mathbf{10^{-5}}$

*Mean values with standard deviations are listed for measurements of $n = 8$ for control mice and $n = 10$ for colitis-bearing mice. Numbers in bold indicate *P* values that were statistically significant between the two groups, as indicated.

[a]IAUC values were calculated up to 1 min. *P* values of ≤0.0005 are considered to be statistically significant.

n.a. - not applicable.